

Received 21 February 2023, accepted 21 March 2023, date of publication 24 March 2023, date of current version 29 March 2023.

Digital Object Identifier 10.1109/ACCESS.2023.3261561

RESEARCH ARTICLE

Speed Regulation Characteristics of Variable Conductivity-Based Barrel-Type Permanent Magnet Eddy Current Governor

WANG TENG^{1,2,3,4}, WANG ZHENGHUI¹, WU YIPENG¹, AND GUO WENXIAO^{2,3,4}¹China Coal Research Institute, Beijing 100013, China²CCTEG Taiyuan Research Institute Company Ltd., Taiyuan 030006, China³Shanxi Tiandi Coal Mining Machinery Company Ltd., Taiyuan 030006, China⁴China National Engineering Laboratory for Coal Mining Machinery, Taiyuan 030006, China

Corresponding author: Wang Teng (wangteng40@126.com)

This work was supported in part by the Chinese National Key Research and Development Program under Grant 2020YEB1314000; and in part by the Scientific Research Projects of Shanxi Tiandi Coal Mining Machinery Company Ltd., under Grant M2021-MS08.

ABSTRACT In this study, a conductivity-regulated barrel-type permanent magnet eddy current governor is proposed, and a conductor barrel structure scheme consisting of four sections of materials with different conductivities is presented. The torque equation of the barrel-type permanent magnet eddy current governor with the equivalent conductivity as the covariate was established using the separation variable method based on the subdomain model. The equivalent conductivity function was established to obtain the speed regulation characteristics of the governor under a constant torque load, and the calculation method for the governor's transmission efficiency was provided. The influence of the conductivity parameters of the conductor barrel on the speed regulation characteristics was studied by numerical simulation, the influence of the conductivity values of each section of the material on the conductivity function was investigated, the torque equation and conductivity function were verified by three-dimensional electromagnetic finite element simulation, and the direction and distribution of eddy current in conductor layer under different working conditions were simulated. The results show that the structural scheme of the four-segment combined conductor barrel can realize a continuous change in conductivity with the displacement of the magnet disk, thus realizing continuous speed regulation of the constant torque load, and the speed regulation characteristic of the governor is segmented linearly. Compared with the air gap-regulated disk-type permanent magnet eddy current governor, the conductivity-regulated barrel-type permanent magnet eddy current governor has a wider speed regulation range, a lower unloading torque after overload protection, and can start with its maximum torque, thus enabling heavy-load starting of constant torque loads, speed regulation operation, and unloading overload protection of equipment.

INDEX TERMS Constant torque load, permanent magnet eddy current governor, speed regulation characteristics, equivalent conductivity, separation variable method.

I. INTRODUCTION

A significant class of loads in industrial production is constant torque loads, which are frequently observed in the continuous transport machinery used in deep coal mines, including belt conveyors, scraper conveyors, transfer machines, and crushers. Its reliable functioning must adhere

The associate editor coordinating the review of this manuscript and approving it for publication was Diana Leitao¹.

to the following technological specifications: Controllable soft start of heavy load, speed regulation (or load balancing), and unloading overload protection. Permanent magnet eddy current speed control technology is a novel speed control transmission technology that has emerged in recent years. Owing to its remarkable advantages of noncontact, no wear and tear, and being unloaded after overloading [1], it is particularly well suited for soft starting and overload protection. It is only utilized in fans, pumps, and other loads

because it has problems with a low starting torque and small speed regulation range when applied to constant torque loads [2], [3], [4].

The speed regulation characteristics of permanent magnet eddy current drives have been studied in many papers. Reference [5] established the torque calculation model of the permanent magnet eddy current coupler with axial magnetic flux by using layer model theory, pointing out that its torque characteristics have mechanical characteristics similar to those of asynchronous motors and that there are overturning and blocking points, with the blocking point being significantly lower than the overturning point. Reference [6] predicted that the torque characteristics of a disk-type permanent magnet governor with air gap adjustment would be similar to those of asynchronous motor with voltage regulation. References [7], [8] examined the characteristics of the disk-type permanent magnet governor's speed regulation under a constant torque load, with speed ranges of 50 and 200 rpm respectively. Reference [9] also noted that the speed range of the disk-type permanent magnet governor was only 13% and that when the conductor barrel material resistance increased, the governor's overturning torque remained essentially unchanged, while the blocking point increased and the torque characteristics became flexible. Reference [10] investigated the air-gap speed regulation characteristics of a disk-type permanent magnet eddy current coupler with a speed range of only about 1.2 and a blocking point torque of 42% of the maximum torque.

Reference [11] investigated the transmission characteristics of a disk-type permanent magnet eddy current coupler using the separated variable method. The analysis revealed that the conductivity and permeability of the magnetic disk have a significant impact on the slope of the torque characteristics, the slope of the peak, and the peak size. The conductivity of the conductor disk has no impact on the maximum torque value, but does affect the slip to reach the maximum torque value. Reference [12] used the method of separating variables in cylindrical coordinates to analyze the torque characteristics of a barrel-type coupler and noted that the speed characteristics of the barrel-type coupler and disk-type permanent magnet coupler follow the same laws. References [13], [14] established a nonlinear analytical model of a barrel-type permanent magnet eddy current coupler using the equivalent magnetic circuit method, which can effectively deal with material parameters and complex geometric shapes. Reference [15] provided a transient equation for the output torque of an axial flux permanent magnet eddy current governor. Under the situation of a low speed difference, the error of the output torque-speed characteristic is less than 10% using finite element simulation and experimental verification. On this basis, the starting and transient characteristics of the output torque of a permanent magnet governor were investigated. The superiority of the permanent magnet eddy current governor in shock load buffering was demonstrated through theoretical analysis and experimental studies. In all the preceding studies, the torque characteristics were altered

by adjusting the air gap, but the conductivity of the conductor layer material remained constant. There have been no published studies on the eddy current flow characteristics of permanent magnet eddy current drive with variable-conductivity materials.

Therefore, this study proposes a barrel-type permanent magnet eddy current governor structure based on conductivity regulation. Four sections conductors of different conductivities were linked axially to create a conductor barrel with a gradient conductivity. The goal is to increase the governor's heavy-load starting capabilities, broaden the speed regulation range, and provide speed regulation and unloading overload protection during operation.

First, the structure and principle of a permanent magnet eddy-current governor with adjustable conductivity are introduced. A torque characteristic equation with the equivalent conductivity as the parameter and the relationship between the equivalent conductivity and the position function of the magnet disk were derived, and the speed regulation characteristics of the governor based on the position of the magnet disk were obtained. The influence of the change in equivalent conductivity on the transmission characteristics and that of the conductivity of segmented conductor on the change rule of the equivalent conductivity of the conductor barrel were explored using a numerical analysis approach.

II. OPERATING PRINCIPLE OF PERMANENT MAGNET GOVERNOR BASED ON CONDUCTIVITY REGULATION

As shown in Fig. 1, the barrel permanent magnet eddy current governor with gradual conductivity of conductor barrel consists primarily of a conductor rotor, permanent magnet rotor, and control mechanism. The conductor rotor and permanent magnet rotor were coaxially nested, with the conductor rotor fastened to motor-shaft-6, and the permanent magnet rotor fixed to load-shaft-7. The conductor rotor was composed of yoke-cylinders-1 and conductor-cylinder-2 inserted into yoke-cylinder-1. The conductivity of conductor-cylinder-2 steadily decreased along the axial direction, from left to right. Yoke-disk-5 and permanent-magnets-4 implanted in the circle of yoke-disk-5 constitute the permanent magnet rotor. Permanent-magnets-4 is alternatively magnetized in the radial direction by N-S poles and positioned uniformly around the circumference. The permanent magnet rotor can move axially along load-axis-7 owing to control-mechanism-8.

When the motor turns, the rotor of the conductor turns. The magnetic force line created by permanent-magnets-4 on the permanent magnet rotor is continually severed by conductor-cylinder-2 on the conductor rotor (Fig. 2). An eddy current occurred in conductor-cylinder-2. Eddy current causes an induced magnetic field to form around conductor-cylinder-2. The magnetic field of permanent-magnets-4 interacts with the induced magnetic field on the conductor rotor, causing the permanent magnet rotor to revolve delayed in the same direction as the conductor rotor and to drive the load output shaft. Control-mechanism-8 can control and alter the axial coupling

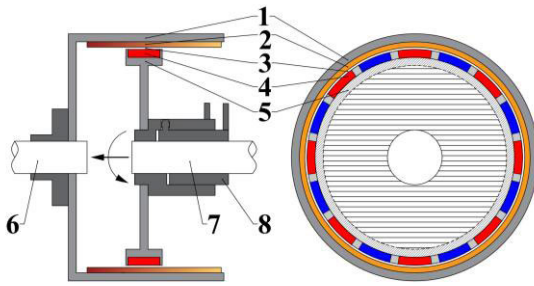


FIGURE 1. Structure of variable impedance conductor barrel-magnet disk.

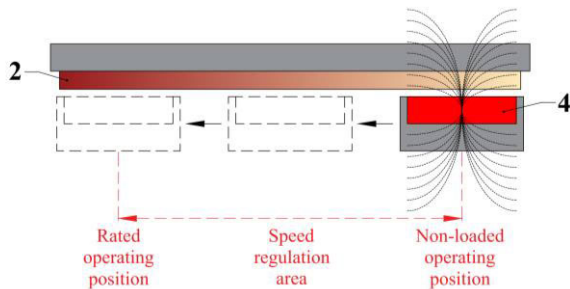


FIGURE 2. Change in axial working position of governor.

point between the permanent magnet rotor and conductor rotor to adjust conductivity and speed.

Fig. 2 shows a close-up of the magnet disk and conductor barrel engagement area shown in Fig. 1. Load start-up, speed regulation, rated operation, and overload protection are the primary functions of a permanent magnet eddy current governor. Fig. 2 shows the position shift of a magnet disk (permanent magnet rotor) during operation. When the motor is not started or is not operating under a load, the permanent magnet rotor is in the no-load operation position, the governor is in the no-load condition, and there is no torque transfer between the input and output shafts. The control mechanism causes the permanent magnet rotor to move to the left, and the conductivity of the conductor cylinder within the magnet disk coverage increases progressively. The equivalent conductivity of the conductor rotor in the coupling section determines the transmission properties of the governor. With the starting torque progressively increased, the load starts when the starting torque is greater than or equal to the load torque (characteristic curve-1 in Fig. 3). When the permanent magnet rotor barely enters the coverage region of the conductor barrel, the starting torque reaches its maximum value (the overturning point of the torque characteristic, curve-2 in Fig. 3). The equivalent conductivity of the conductor barrel coupling section increased as the permanent magnet rotor continued to travel to the left under the control mechanism. When the governor eventually reaches the limit position, it enters the rated operation state (characteristic curve-3 in Fig. 3 and the rated operation position in Fig. 2).

When a sudden overload occurs at the load end during rated governor operation, the slip between the primary-

secondary ends increases significantly. At this point, the governor's working point quickly exceeds the maximum torque point B from the rated working point A to the locked rotor point C, and the locked rotor torque is very small, resulting in motor and transmission system overload protection (as shown in Fig. 3).

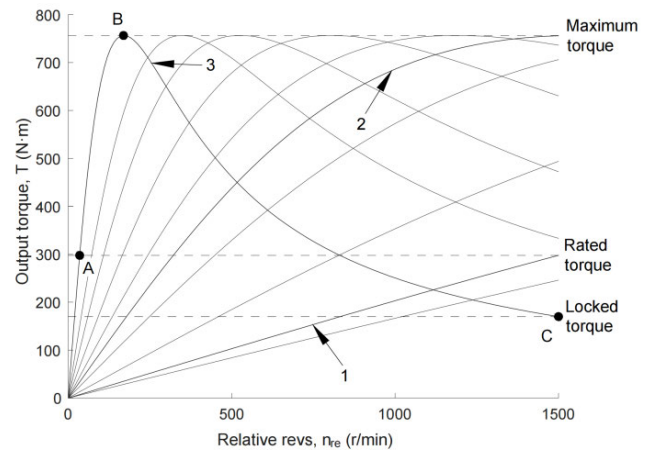


FIGURE 3. Change of transmission characteristic curve of permanent magnet eddy current governor.

III. TRANSMISSION CHARACTERISTIC OF GOVERNOR

The magnetic field distribution and electromagnetic torque of the governor must be precisely calculated to investigate the speed control performance of the permanent magnet eddy current governor. First, the conductor cylinder area covered by the permanent magnet at each axial position on the magnet disk is treated as if it were a material with equivalent single conductivity, and the separated variable method was applied to the three-dimensional eddy current field of the barrel-type permanent magnet eddy current governor to establish the governor's transient torque calculation model. Second, the equivalent conductivity of the covered area is computed using the loop resistance equivalence principle, and the obtain torque equation is replaced to produce speed regulation characteristics that vary with the location of the magnet disk.

A. STRUCTURE AND PARAMETER DESIGN OF CONDUCTOR BARREL

To achieve axial variation in the conductivity of the conductor barrel, the conductor barrel was built in four parts as a combination of materials with different conductivities (Fig. 4). As shown in Fig. 5, Section-A relates to the conductivity under no-load operating condition, section-D corresponds to the conductivity under rated working condition, and Section-B and Section-C are conductive transition sections. When the magnet disk position corresponds to the conductor of Section-B, the governor's start torque meets the rated torque, and Section-C is utilized to coordinate the speed control process to smoothly transfer the governor speed to Section-D. Section-D's conductivity is dictated by the power



FIGURE 4. Three-dimensional structure of Segmented conductor barrel-magnet disk.

and cannot be set randomly. The conductivities value of Section-B and Section-C can be freely chosen between the conductivity ranges of sections-A and Section-D to replicate various gradual change laws of conductivity.

Fig. 5 and Fig. 6 show the axial and radial coupling diagrams of the conductor barrel and the magnetic disk, respectively. Conductivities of conductor barrel segments A, B, C, and D were $\sigma_1, \sigma_2, \sigma_3,$ and $\sigma_4,$ respectively. Their value corresponds to the following relationship: $\sigma_1 > \sigma_2 > \sigma_3 > \sigma_4.$

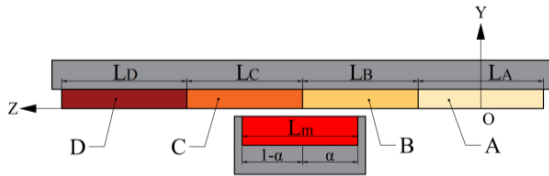


FIGURE 5. Axial section of coupling part of governor.

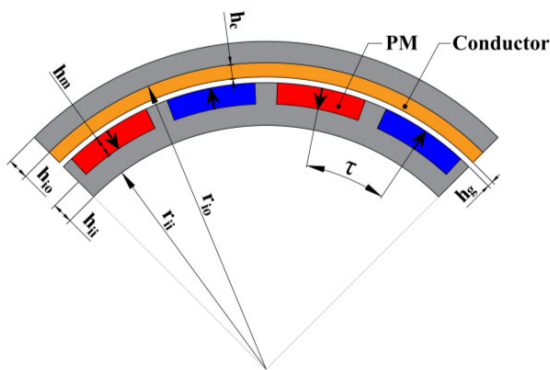


FIGURE 6. Radial section of coupling part of governor.

B. LAYER MODEL OF MAGNETIC FIELD AND ITS BASIC ASSUMPTIONS

We assume that the cylindrical permanent magnet eddy current governor model is expanded into a linear model along its circumference [16] and that the model is axially truncated to generate a two-dimensional linear model in the Cartesian

coordinate system (Fig. 7). The transformed 2D linear model is separated into five layers:

- Layer 1: the outer magnetic yoke layer.
- Layer 2: solid conductor layer.
- Layer 3: air gap layer.
- Layer 4: permanent magnet layer.
- Layer 5: inner yoke layer.

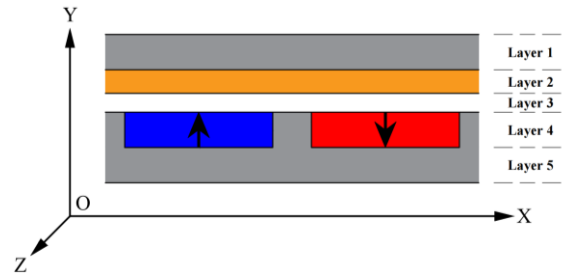


FIGURE 7. Two-dimensional linear model in Cartesian coordinate system.

The following assumptions are established to simplify the calculating procedure and facilitate the study:

- 1) Considering only the vortex component in the z-direction, since only the z-direction vortex component contributes to the torque of the governor;
- 2) Assume that the yoke iron’s conductivity is 0 and disregard the yoke iron’s eddy current loss;
- 3) Ignoring the conductor layer’s displacement current;
- 4) Ignoring the presence of the inner yoke iron in the permanent magnet layer and assume it has the same permeability as the permanent magnet;
- 5) Ignoring the curvature error due to the transformation of the coordinate system;
- 6) The model has a natural period boundary condition along the x-direction, with the period determined by the pole spacing of the permanent magnets;
- 7) Assume that the conductor barrel and outer yoke are “fixed,” and that the permanent magnets and inner yoke rotate with velocity Δv relative to the conductor rotor (Δv is the slip line velocity at the equivalent radius r_c of the conductor barrel, $r_c = r_{io} - h_c/2$).

The transient torque calculation model of the barrel-type permanent magnet eddy current governor was analyzed using the aforementioned assumptions.

C. BASIC CONTROL EQUATIONS OF MAGNETIC FIELD AND VECTOR MAGNETIC POTENTIAL DISTRIBUTION

The basic equation of magnetic field stated in terms of the vector magnetic potential \mathbf{A}_k is (see Appendix A for the derivation):

$$\nabla^2 \mathbf{A}_k = -\mu_0 (\mu_k \nabla \times \mathbf{H}_k + \nabla \times \mathbf{M}_k) \tag{1}$$

In (1), k represents the layer number, \mathbf{H}_k represents the strength of the magnetic field of the k th layer, \mathbf{M}_k represents the magnetization of the k th layer, and μ_0 and μ_k represent

the vacuum permeability and relative permeability of the k th layer material respectively.

Layer 4: The magnetic field of the governor is excited by permanent magnets on the magnet disk. The permanent magnet area is a rotating passive field with a y -direction component B_{4y} of magnetic induction \mathbf{B}_4 presents a periodic rectangular wave along the x -direction with an alternating configuration of N-pole and S-pole permanent magnets (Fig. 8), whose values are B_r and $-B_r$ inside the permanent magnets and 0 outside the permanent magnets. When expressed as a Fourier series, it has the following formula:

$$B_{4,y} = \sum_n e^{imx} B_r, \quad m = \frac{\pi}{\tau} n, \quad (n = \pm 1, \pm 3, \pm 5 \dots) \quad (2)$$

In (2), τ is the pole-angle spacing (Fig. 6).

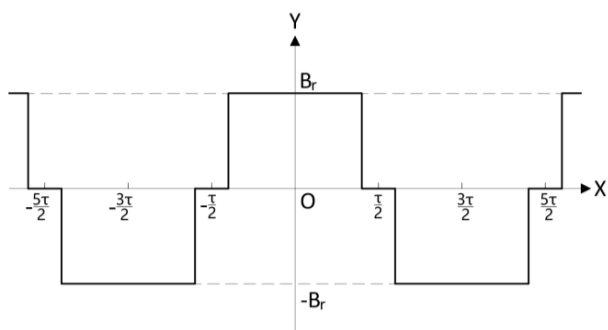


FIGURE 8. Change of magnetic induction in the y -direction along the x -direction (Layer 4).

Based on assumption 1), considering only the eddy current component J in the z -direction means taking into account only the vector magnetic potential A_z in the z -direction, and the strength of the magnetic field H and magnetic induction B in the z -direction are ignored because only the strength of the magnetic field and magnetic induction originating from the x - and y -directions contribute to the vector magnetic potential in the z -direction.

The vector magnetic potential of each layer can be expressed using the separated variables method as follows:

$$A_k(x, y) = A_k(x) \cdot A_k(y) \quad (3)$$

According to assumption 6), the electromagnetic field of the model is periodic along the x -direction and then in the permanent magnet layer:

$$A_4(x, y) = \sum_n e^{imx} \cdot A_4(y) \quad (4)$$

The permanent magnet layer's basic magnetic field equation was deduced [12], and we obtain:

$$\frac{\partial^2 A_4(y)}{\partial y^2} - m^2 A_4(y) = -imB_r \quad (5)$$

Layer 1, 3, 5: According to assumption 2), there is no current in the air gap and the inner and outer yoke iron, and

the corresponding basic equation of magnetic field is:

$$\nabla^2 A_k = \frac{\partial^2 A_k}{\partial x^2} + \frac{\partial^2 A_k}{\partial y^2} = 0 \quad (6)$$

In (6), $k = 1, 2, 3$.

Layer 2: There is no magnetization M in the conductor layer, and the basic equation of magnetic field is:

$$\nabla^2 \mathbf{A}_2 = -\mu_0 \mu_2 \nabla \times \mathbf{H}_2 \quad (7)$$

According to assumption 3), at a low slip speed, when the displacement current is ignored and only the induced eddy currents in the conductor layer are considered, the basic equation of magnetic field in the conductor layer was reduced using basic electrodynamics knowledge [12], and we obtained that:

$$\frac{\partial^2 A_{2,y}}{\partial y^2} - (m^2 + im\mu_0 \mu_2 \sigma_c \Delta v) A_{2,y} = 0 \quad (8)$$

By solving (5), (6), and (8), the vector magnetic potential of each layer can be obtained as follows [17], [18], [19]:

$$\begin{cases} A_1 = (C_1 e^{my} + D_1 e^{-my}) e^{imx} \\ A_2 = (C_2 e^{\lambda y} + D_2 e^{-\lambda y}) e^{imx} \\ A_3 = (C_3 e^{my} + D_3 e^{-my}) e^{imx} \\ A_4 = \left(C_4 e^{my} + D_4 e^{-my} - \frac{iB_r}{m} \right) e^{imx} \\ A_5 = (C_5 e^{my} + D_5 e^{-my}) e^{imx} \end{cases} \quad (9)$$

In (9), the coefficients C_k and D_k are derived using the model boundary conditions, and λ is calculated using the open square calculation of complex numbers [20]:

$$\begin{cases} \lambda = \sqrt[4]{m^4 + (m\mu_0 \mu_2 \sigma_c \Delta v)^2} e^{\delta} \\ \delta = \frac{i}{2} \arctan \left(\frac{\mu_0 \mu_2 \sigma_c \Delta v}{m} \right) \end{cases} \quad (10)$$

D. BOUNDARY AND INTERFACE CONDITIONS

To the model, add the Dirichlet boundary condition:

$$\begin{cases} A_1|_{y=+\infty} = 0 \\ A_5|_{y=-\infty} = 0 \end{cases} \quad (11)$$

And Dirichlet and Neumann interface condition:

$$\left. \begin{aligned} \frac{dA_k}{dx} &= \frac{dA_{k+1}}{dx} \\ \frac{1}{\mu_k} \frac{dA_k}{dy} &= \frac{1}{\mu_{k+1}} \frac{dA_{k+1}}{dy} \end{aligned} \right|_{y=r_{io}, r_{ic}, r_{ig}, r_{im}}, \quad k = 1, 2, 3, 4 \quad (12)$$

In (12), r_{io} is the inner radius of the outer yoke layer, r_{ic} is the inner radius of the conductor layer, r_{ig} is the inner radius of the air gap layer, and r_{im} is the inner radius of the permanent magnet layer.

Appendix B shows the detailed form of the boundary conditions.

E. EDDY CURRENT LOSS AND TORQUE

Because of the presence of slip during governor operation, the induced eddy current magnetic field created by the induced eddy current in the conductor layer interacts with the permanent magnet magnetic field to transfer force from the active end to the driven end, resulting in torque transmission. The magnetic field's work is equal to the conductor layer's heat loss power P_{loss} , which comprises end loss P_{ξ} and slip loss P_{ω} :

$$P_{loss} = P_{\xi} + P_{\eta} \tag{13}$$

In the conductor layer, the eddy current density is:

$$J_2 = \sum_n -\sigma_c \Delta v \frac{dA_2}{dx} \tag{14}$$

The slip loss in the corresponding conductor layer when the magnet disk is entirely covered by the conductor barrel is computed from the eddy current density, as P_{ω} :

$$P_{\omega} = \frac{L_m}{\sigma_c} \iint_{Layer\ 2} |J_2^2| dx dy \tag{15}$$

If the end loss P_{ξ} is ignored, the torque T delivered by the governor can be approximated as follows:

$$T = \frac{P_{\omega}}{\Delta\omega} \tag{16}$$

In (16), $\Delta\omega$ denotes the angular velocity difference between the conductor barrel and magnet disk, $\Delta\omega = \frac{\Delta v}{r_c} = \frac{2\pi n_{re}}{60}$, and n_{re} denotes the slip speed between the conductor barrel and magnet disk.

F. EQUIVALENT CONDUCTIVITY

The calculation method for the equivalent conductivity of the coupling part of the conductor layer was described using Section-B and Section-C of the barrel section as examples. Fig. 9 shows the circumferential plane of the connecting portion. The eddy current path is depicted in green, whereas the permanent magnets and their impacted areas are depicted in blue (N-pole) and red (S-pole), respectively. Because the end loss is ignored in (16), the end resistance is 0. Fig. 10 shows the corresponding circuit on the eddy current channel. The equivalent conductivity of the coupling portion is computed using an equivalent circuit.

In Fig. 9, α represents the ratio of the coupling part of the Section-B with the permanent magnets to the axial length of the permanent magnet; L_p represents the width of the eddy current spillover in the conductor layer (Fig. 9), and $L_p = \gamma L_m$.

R_{z1} , R_{z2} , R_{z3} , and R_{z4} in Fig. 10 correspond to the resistances of Section-B and Section-C in the vortex circuit in Fig. 9.

According to the definition of conductivity of a conductor $\sigma = \frac{L}{RS}$, the conductor resistance is computed using the following formula:

$$R = \frac{L}{\sigma S} \tag{17}$$

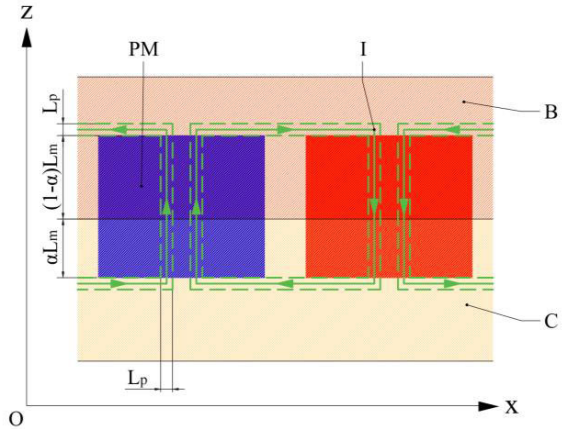


FIGURE 9. Plane expansion of eddy current path.

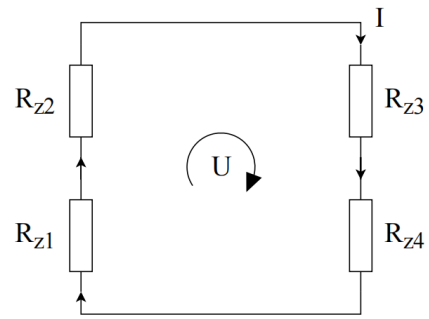


FIGURE 10. Equivalent circuit of conductor layer.

In (17), L is the length of the vortex flow through the conductor and S is the cross-sectional area of the vortex flow through the conductor.

Write the expression for each equivalent resistance in Fig. 10:

$$\begin{cases} R_{z1} = \frac{\alpha_2 L_m}{\sigma_2 S_{z1}} \\ R_{z2} = \frac{(1 - \alpha_2) L_m}{\sigma_3 S_{z2}} \\ R_{z3} = \frac{(1 - \alpha_2) L_m}{\sigma_3 S_{z3}} \\ R_{z4} = \frac{\alpha_2 L_m}{\sigma_2 S_{z4}} \end{cases} \tag{18}$$

Given that the spillover width L_p is substantially smaller than that of the permanent magnet, the effective cross-sectional area of the eddy current flowing through each resistor is considered to be the same:

$$S_E = S_{z1} = S_{z2} = S_{z3} = S_{z4} = L_p \times h_c \tag{19}$$

In (19), h_c is the conductor layer thickness (Fig. 6) and S_{zi} is the area of the through-flow section corresponding to R_{zi} ($i = 1-4$).

The entire equivalent circuit resistance R_E can be computed using the series equation of resistance, as follows:

$$\begin{aligned}
 R_E &= R_{z1} + R_{z2} + R_{z3} + R_{z4} \\
 &= \frac{\alpha_2 L_m}{\sigma_2 S_{z1}} + \frac{(1 - \alpha_2) L_m}{\sigma_3 S_{z2}} + \frac{(1 - \alpha_2) L_m}{\sigma_3 S_{z3}} + \frac{\alpha_2 L_m}{\sigma_2 S_{z4}} \\
 &= \frac{2L_m [(1 - \alpha_2) \sigma_2 + \alpha_2 \sigma_3]}{\sigma_2 \sigma_3 S_E} \tag{20}
 \end{aligned}$$

Ignoring the equivalent current in the x-direction of the equivalent current and the length of its inflection point, the total equivalent current path length L_E is:

$$L_E = 2L_m \tag{21}$$

According to the definition of conductivity, the equivalent conductivity $\bar{\sigma}$ of the conductor layer in the coupling section is obtained when the permanent magnet crosses the conductors in Section-B and Section-C by means of the simultaneous (18)-(21):

$$\bar{\sigma} = \frac{L_E}{R_E S_E} = \frac{\sigma_2 \sigma_3}{(1 - \alpha_2) \sigma_2 + \alpha_2 \sigma_3} \tag{22}$$

The equivalent conductivity of the entire conductor barrel region along the axial direction was calculated using the method described above:

$$\bar{\sigma}(z) = \begin{cases} \sigma_1, & 0 \leq z < L_p; \\ \frac{\sigma_1 \sigma_2}{(1 - \alpha_1) \sigma_1 + \alpha_1 \sigma_2}, & L_p \leq z < L_B + L_p; \\ \frac{\sigma_2 \sigma_3}{(1 - \alpha_2) \sigma_2 + \alpha_2 \sigma_3}, & L_B + L_p \leq z < L_B + L_C + L_p; \\ \frac{\sigma_3 \sigma_4}{(1 - \alpha_3) \sigma_3 + \alpha_3 \sigma_4}, & L_B + L_C + L_p \leq z < L_B + L_C + L_D - L_p; \\ \sigma_4, & L_B + L_C + L_D - L_p \leq z \leq L_B + L_C + L_D + L_p. \end{cases} \tag{23}$$

In (23), α_1 , α_2 , and α_3 of the following expression:

$$\begin{cases} \alpha_1 = 1 - \frac{z - L_p}{L_m}, & L_p \leq z < L_B + L_p; \\ \alpha_2 = 1 - \frac{z - (L_B + L_p)}{L_m}, & L_B + L_p \leq z < L_B + L_C + L_p; \\ \alpha_3 = 1 - \frac{z - (L_B + L_C + L_p)}{L_m}, & L_B + L_C + L_p \leq z < L_B + L_C + L_D - L_p. \end{cases} \tag{24}$$

G. THREE-DIMENSIONAL END EFFECT

As shown in Fig. 11, the induced eddy current exists in the conductor as a closed loop; however, only the eddy current flowing in the axial direction affects the torque of the governor. Therefore, (16) ignores the circumferential flow of eddy current outside the engagement region of the permanent magnet and conductor layer, but the three-dimensional end effect caused by its effect on the density of eddy current flowing in

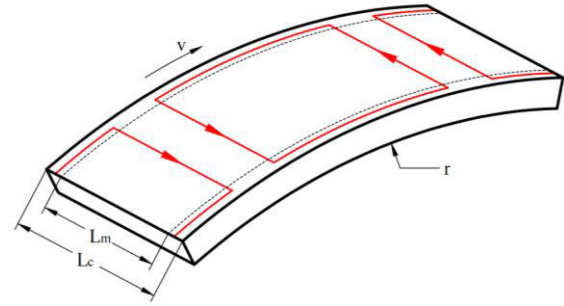


FIGURE 11. Eddy current path.

the axial direction cannot be ignored. Thus, end effect correction is needed for the above analytical results. Reference [21] provided a correction factor that considers three-dimensional end effects to improve the torque computation accuracy of the model. Eddy current losses are apportioned throughout the eddy-current circuit by altering the conductivity of the conductors. The conductor layer conductivity difference at the two ends of the magnet disk can be ignored for the segmented barrel-type permanent magnet eddy current governor studied in this paper and the equivalent conductor barrel conductivity corresponding to the magnet disk is used to calculate the correction factor, which is specified as:

$$K_s = 1 - \frac{\tanh\left(\frac{\rho L_m}{2r_c}\right)}{\left(\frac{\rho L_m}{2r_c}\right) \left[1 + \tanh\left(\frac{\rho L_m}{2r_c}\right) \tanh\left(\gamma \frac{\rho L_m}{r_c}\right)\right]} \tag{25}$$

Equivalent conductivity $\bar{\sigma}(z)$ replaces the conductivity σ_c of the conductor layer. All of the preceding calculations result in the following torque calculation formula for the barrel-type permanent magnet eddy current governor:

$$\begin{aligned}
 T' &= K_s T \\
 &= K_s \bar{\sigma}(z) pm \Delta \omega r_c^2 L_m \iint_{Layer2} |A_2^2| dx dy \tag{26}
 \end{aligned}$$

H. SPEED REGULATION CHARACTERISTICS OF GOVERNOR

When using the governor for a constant torque load, the load constant C is maintained; that is, $T' = C$. Combining the variation of the equivalent conductivity with the magnet disk displacement z and transforming (26), the relationship between the output speed n_{out} and the magnet disk displacement z of the barrel-type permanent magnet eddy current governor under a constant torque load can be determined as follows:

$$n_{out} = n_{in} - \frac{30C}{\pi K_s \bar{\sigma}(z) pm r_c^2 L_m \iint_{Layer2} |A_2^2| dx dy} \tag{27}$$

In (27), n_{in} is the input speed of the motor.

The governor is a constant torque transmission mechanism, which means that the input torque M_{out} equals the output

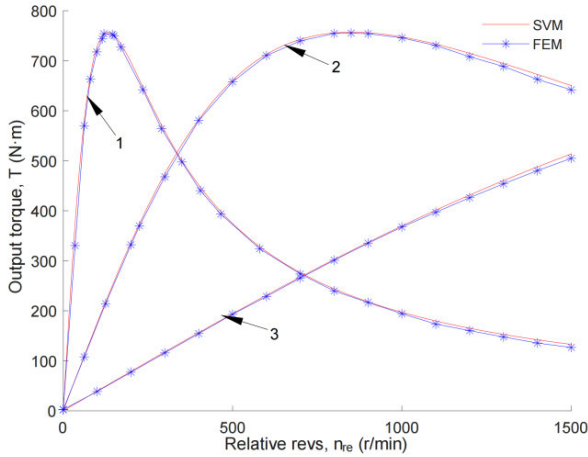


FIGURE 12. Finite element analysis of transmission characteristics of speed governor with different conductivity.

torque M_{in} , and the governor’s transmission efficiency is computed as η :

$$\eta = \frac{P_{out}}{P_{in}} = \frac{M_{out} (2\pi n_{out}/60)}{M_{in} (2\pi n_{in}/60)} = \frac{n_{out}}{n_{in}} \quad (28)$$

IV. VERIFICATION OF TORQUE CALCULATION MODEL BY FINITE ELEMENT METHOD ANALYSIS

In order to verify the accuracy of the proposed theory of permanent magnet eddy current speed regulation, the three-dimensional finite element method (FEM) analysis was carried out according to the specifications of barrel-type permanent magnet eddy current governors given in Table 1 and Table 2.

The coupling model of cylinder-magnet disk with single material was established, and conductor conductivity of different layers was set up separately. Finite element simulation was carried out. The generated scatter plot was compared with the transmission characteristic curves generated by the transient torque calculation model established by the separation variable method (SVM) under the same conditions.

Curves 1, 2, and 3 in Fig. 12 correspond to conductor layer conductivities of 58×10^6 S/m, 9×10^6 S/m, and 2×10^6 S/m respectively. The torque computed by the theoretical model in this study and the simulation results of the finite element approach largely match in the region of speed difference of 0-1000 rpm. The maximum torque inaccuracy is less than 5% in the speed difference range of 1000-1500 rpm. The source of the error is primarily the parameter setting of the finite element model and the transformation of the aforementioned transient torque calculation model from a 3D cylindrical model to a 2D linear model. Given that this error is within the allowable range of engineering design, the separation variable method used in this study can be used for the analysis of the governor transmission characteristics.

TABLE 1. Structural characteristics of governor.

Symbol	Definition	Values
r_{ii}	inner radius of the inner magnetic yoke	171 mm
r_{io}	inner radius of the outer magnetic yoke	213 mm
h_{ii}	thickness of inner yoke	15 mm
h_m	Thickness of permanent magnets	15 mm
h_g	thickness of air gap	2 mm
h_c	thickness of conductor layer	10 mm
h_{io}	thickness of outer yoke	15 mm
L_A	axial length of conductor barrel section A	65 mm
L_B	axial length of conductor barrel section B	60 mm
L_C	axial length of conductor barrel section C	60 mm
L_D	axial length of conductor barrel section D	65 mm
L_m	axial length of permanent magnets	60 mm
α	duty cycle of permanent magnets	0.8
p	polar number	16
n_{in}	input speed	1500 rpm

TABLE 2. Material properties.

Symbol	Definition	Values
μ_0	permeability of vacuum	$4\pi \times 10^{-7}$ Tm/A
μ_1	relative permeability of outer yoke iron layer and permanent magnet pole spacer material (stainless steel)	1
μ_2	relative permeability of the conductor layer	1
μ_3	Relative permeability of the air layer	1
μ_4	Relative permeability of the permanent magnet layer (NdFeB35)	1.0997785406
H_c	Coercivity of permanent magnet layer (NdFeB35)	-8.9×10^5 A/m
μ_5	Relative permeability of the inner yoke iron layer (1008 steel)	1200

V. ANALYSIS AND DISCUSSION

A. EFFECT OF CHANGE IN CONDUCTIVITY ON TRANSMISSION CHARACTERISTICS OF GOVERNOR

The effect of change in conductivity on transmission characteristics of governor was analyzed. Based on the parameters in Table 1 and Table 2, the coupling model of conductor barrel of single material-magnet disk is designed. The conductivity of conductor barrel is set from 0- 58×10^6 S/m, and the numerical simulation is carried out by (26). The results of several characteristic curves are shown in Fig. 13.

In the field of engineering design, 1/2.5 of the overturning point torque T_{max} is generally taken as the rated load torque T_e . Therefore, the load values were taken as T_{max} (756 N·m), $1.2T_e$ (363 N·m), T_e (302 N·m), and $0.5T_e$ (151 N·m), and their load lines are drawn in Fig. 13.

As shown in Fig. 13, as the conductivity changes, the governor’s transmission characteristics are characterized by the following properties:

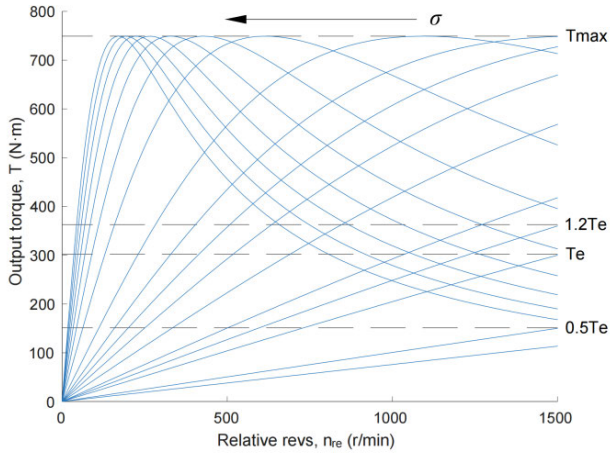


FIGURE 13. Effect of conductivity change on transmission characteristics of governor.

- 1) The overturning point torque of the transmission characteristic of the governor does not change with the conductivity and is a fixed value.
- 2) With the decrease of conductivity, the transmission characteristic curve changes from hard to soft.
- 3) After full startup, the blocking point torque (speed difference is 1500 rpm) of the governor decreases with increasing conductivity.

It can be concluded that conductivity regulation can achieve:

- 1) Maximum starting torque ($2.5T_e$) can be achieved by utilizing the overturning point of the transmission characteristics to achieve heavy load starting.
- 2) Achieving speed regulation start and operation of load, the theoretically achievable speed regulation range $0 \sim n_e$ (n_e is the rated speed) is much larger than that of the permanent magnet speed regulator with air gap regulation.
- 3) Unloading overload protection is realized, and the drive torque after unloading is only approximately $0.5 T_e$, which effectively protects the transmission system and reduces the heating power of the governor.

The changes in the governor's output speed $n_{out} = n_{in} - n_{re}$ corresponding to the varying conductivities at load T_{max} , $1.2T_e$, T_e , and $0.5T_e$ are plotted in Fig. 14. It can be seen that when the conductivity increases, so does the output speed, but the lifting speed decreases, indicating that the connection between the output speed and conductivity is nonlinear.

B. ANALYSIS OF VARIATION RULE OF EQUIVALENT CONDUCTIVITY

It is necessary to investigate the influence law on the equivalent conductivity when different conductivity materials are set in the conductor barrel segments to design the speed regulation characteristics of the permanent magnet eddy current

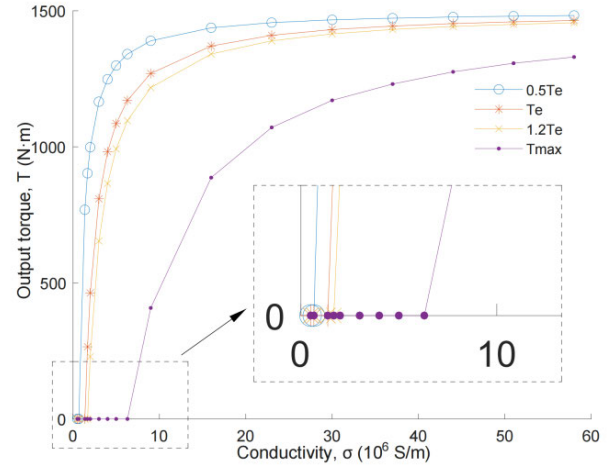


FIGURE 14. Variation of output speed with conductivity under different loads.

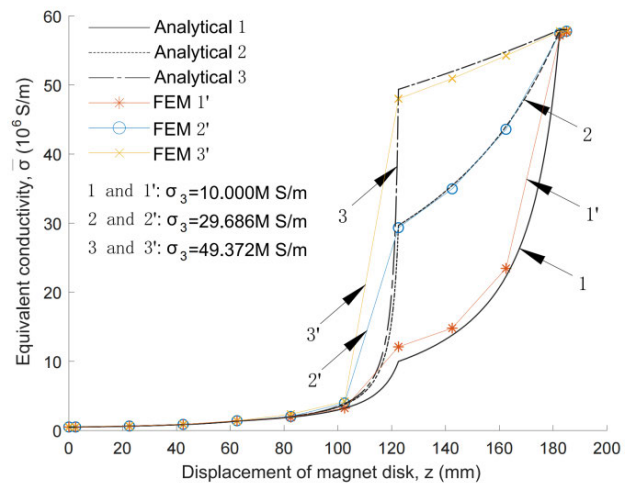


FIGURE 15. Comparison between analytical and FE computation of three equivalent conductivity variation rules.

governor with the segmented conductor barrel proposed in this study. The conductivity of Section-A in Fig. 5 is that of no load, whereas the conductivity of Section-D is that of pure copper. To alter the speed regulation characteristics, only the conductivities of Section-B and Section-C can be modified freely. To reflect the speed change law of the rated torque, the conductivity of Section-B was configured to correspond to the conductivity value σ_2 when the governor blocking point torque was T_e . Fig. 14 shows that the link between speed and conductivity change is faster than slower. Therefore, the conductivity setting follows the following principle:

$$\sigma_4 - \sigma_3 > \sigma_3 - \sigma_2 \quad (29)$$

To confirm (29), the axial length of the permanent magnet $L_m = 60$ mm, $\sigma_1 = 0.5 \times 10^6$ S/m, $\sigma_4 = 58 \times 10^6$ S/m, the conductivity value of the Section-B was set to the conductivity corresponding to the starting torque T_e , that is, $\sigma_2 = 1.372 \times 10^6$ S/m, and the conductivity value of the Section-C

was set to the following three cases and verified by finite element simulation (Fig. 15):

1) INCREMENTAL RATE FIRST SMALL THEN LARGE PRINCIPLE

The increase rate of equivalent conductivity of conductor barrel with the displacement of magnet disk is small first and then large. Taking $\sigma_3 = 10^7$ S/m, we obtain:

$$(\sigma_3 - \sigma_2 = 8.628) < (\sigma_4 - \sigma_3 = 48)$$

2) INCREMENTAL RATE CONSTANCY PRINCIPLE

Conductor barrel conductivity increases at a constant rate with the displacement of the magnet disk. Take $\sigma_3 = \frac{\sigma_4 + \sigma_2}{2} = 29.686 \times 10^6$ S/m, we obtain:

$$(\sigma_3 - \sigma_2 = 28.314) = (\sigma_4 - \sigma_3 = 28.314)$$

3) INCREMENTAL RATE FIRST LARGE THEN SMALL PRINCIPLE

The increase rate of equivalent conductivity of conductor barrel with the displacement of magnet disk is large first and then small. Taking $\sigma_3 = 49.372 \times 10^6$ S/m, we obtain:

$$(\sigma_3 - \sigma_2 = 48) > (\sigma_4 - \sigma_3 = 8.628)$$

Fig. 15 shows the distance from the no-load section to the left of the magnet disk. Zero cross-coordinates indicate that the magnet disc is in the no-load section, 62.5 mm indicates that the magnet disk is in Section-B, 122.5 mm indicates that it is in Section-C and 185 mm indicates that it is in Section-D. The ordinates represent the equivalent conductivity.

Fig. 15 shows that:

- 1) Curve-1 in the conductor barrel in Section-C is smoother than curve-2 and curve-3;
- 2) The three curves show a gentle change between Section-B and Section-C (62.5-122.5 mm), while a sharp change between Section-C and Section-D (122.5-185 mm), especially curve-1;
- 3) The theoretical analysis results are in good agreement with the finite element analysis results.

According to the variation rule of speed-conductivity curves in Fig. 14, the gradient of conductivity-displacement curve should be slow-first-then-fast in order to obtain approximate linear speed-regulating characteristics. From this analysis, it can be seen that the setting of conductor barrel Section-C with conductivity close to curve-1 will make the governor have better speed regulation performance.

C. SPEED REGULATION CHARACTERISTICS OF CONSTANT TORQUE LOAD

Based on these findings, the conductivity of conductor barrel Section-C was set to 10^7 S/m, and the rated load torque T_e was set at 1/2.5 of the overturning point torque T_{max} . The transmission characteristics of the magnet disk as it moves from right to left are calculated using (26) (Fig. 16), and the speed values when the load is T_e , $1.2T_e$, and $0.5T_e$ are

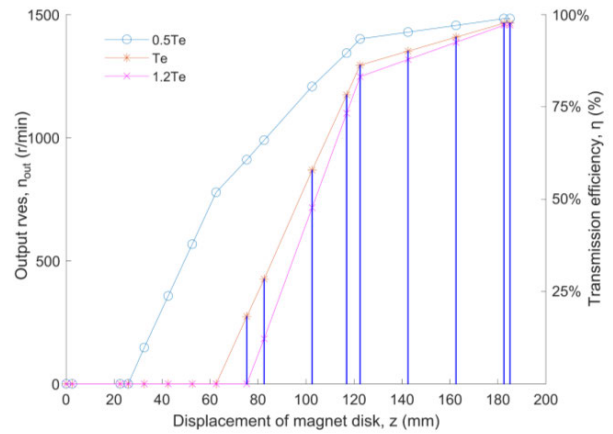


FIGURE 16. Speed regulation characteristics of governor ($n_{out} - z$) and transmission efficiency of governor.

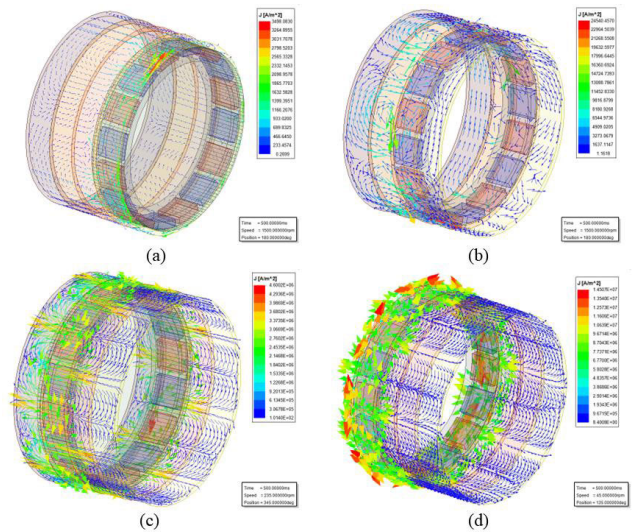


FIGURE 17. Eddy current density vector of conductor layer.

derived from (27), that is, the change of output speed during the whole process from startup to stable operation of the governor. Fig. 16 shows the $z-n_{out}$ curve. The speed governor was simulated and analyzed. The eddy current density vector and eddy current distribution of the conductor layer at different locations is shown in Fig. 17 and Fig. 18.

Fig. 16 shows that when the load was changed, the speed regulation characteristics changed slightly. The length of the part where the speed of the initial section was zero was the difference. The displacement of the magnet disk required to start the load increased as the constant-torque load value increased. The larger the load, the longer the zero-speed interval. This is due to the fact that the governor's transmission torque increases from no-load torque to load torque as the magnet disk moves. After the governor is started, because the change rate of conductivity appropriately compensates for the nonlinearity of the speed change, the governor's speed regulation characteristic is approximately piecewise linear, and the linear speed regulation characteristic is convenient

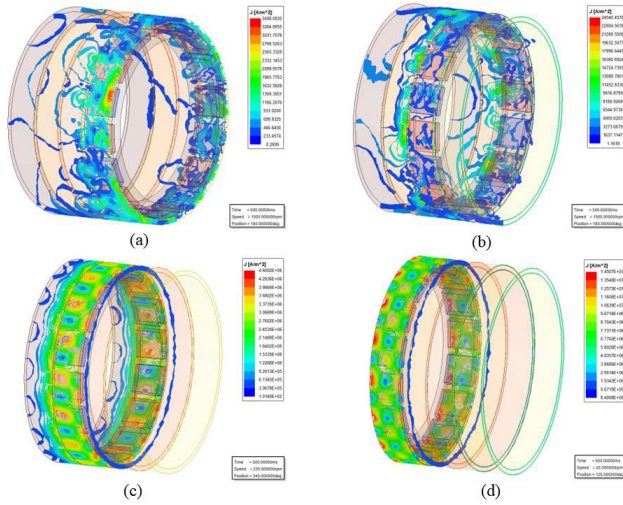


FIGURE 18. Eddy current distribution of conductor layer.

for the control algorithm design. With the gradual start-up of the governor, the equipment transfer efficiency gradually increases from zero to maximum. As shown in Fig. 17 and Fig. 18, (a), (b), (c), and (d) correspond to the distribution of eddy current in the conductor layer when the position of the magnet disc is 0 mm, 62.5 mm, 122.5 mm, and 185 mm. It can be seen from the diagram that the density of eddy current in the conductor layer becomes higher and higher from no-load starting to stable operation of the governor, and the power transmitted by the governor also increases gradually, which conforms to the theoretical results.

VI. CONCLUSION

- 1) The use of a permanent magnet eddy current governor with conductivity adjustment was proposed. The four-section combined conductor cylinder structure design enables no-load beginning, speed regulating soft starting, speed regulating for constant torque load, and unloading overload prevention.
- 2) The conductivity of the conductor barrel changes its transmission characteristics. When the conductivity decreases, the overturning torque of the transmission characteristics remains constant, the blocking point drops, and the transmission characteristics change from hard to soft.
- 3) The torque characteristic equation and equivalent conductivity calculation formula, with the equivalent conductivity as the parameter variable, were established using the separation-of-variables approach. The numerical analysis results of these formulas were mostly consistent with the finite element analysis results.
- 4) The sectional structure can realize the gradual change of conductivity of the conductor layer during the speed regulation process. Except that the conductivity of the starting section and the rated operation section should be set in advance, the conductivity value of the speed regulation section can be set as required to

flexibly design the speed regulation characteristics of the governor.

APPENDIX A

The basic equation of magnetic field is:

$$\mathbf{B}_k = \mu_0 \mu_k \mathbf{H}_k + \mu_0 \mathbf{M}_k \quad (30)$$

The three-dimensional eddy current magnetic field of a permanent magnet eddy current governor is a revolving field that contains the following:

$$\nabla \times \mathbf{B}_k = \mu_0 (\mu_k \nabla \times \mathbf{H}_k + \nabla \times \mathbf{M}_k) \quad (31)$$

When the vector magnetic potential \mathbf{A} is included, $\mathbf{B} = \nabla \times \mathbf{A}$, implying that:

$$\nabla \times (\nabla \times \mathbf{A}_k) = \mu_0 (\mu_k \nabla \times \mathbf{H}_k + \nabla \times \mathbf{M}_k) \quad (32)$$

The rotation formula of the vector field is:

$$\nabla \times (\nabla \times \mathbf{A}_k) = \nabla (\nabla \cdot \mathbf{A}_k) - \nabla^2 \mathbf{A}_k \quad (33)$$

Substituting (33) and the Coulomb gauge $\nabla \cdot \mathbf{A} = 0$ into (32) yields the basic control equation of magnetic field stated in terms of the vector magnetic potential \mathbf{A} :

$$\nabla^2 \mathbf{A}_k = -\mu_0 (\mu_k \nabla \times \mathbf{H}_k + \nabla \times \mathbf{M}_k) \quad (34)$$

APPENDIX B

Because the analytical equations for the coefficients C_k and D_k are complex and ordinarily difficult to state, this appendix explains how to calculate these coefficients.

First, the Dirichlet boundary condition of (11) can be used to introduce the fact that:

$$\begin{cases} C_1 = 0 \\ D_5 = 0 \end{cases} \quad (35)$$

Then write the Dirichlet and Neumann interface condition for (12) specifically:

$$\begin{aligned} \frac{dA_1}{dx} &= \frac{dA_2}{dx} \Big|_{y=r_{io}} \\ \frac{dA_2}{dx} &= \frac{dA_3}{dx} \Big|_{y=r_{ic}} \\ \frac{dA_3}{dx} &= \frac{dA_4}{dx} \Big|_{y=r_{ig}} \\ \frac{dA_4}{dx} &= \frac{dA_5}{dx} \Big|_{y=r_{im}} \\ \frac{1}{\mu_1} \frac{dA_1}{dy} &= \frac{1}{\mu_2} \frac{dA_2}{dy} \Big|_{y=r_{io}} \\ \frac{1}{\mu_2} \frac{dA_2}{dy} &= \frac{1}{\mu_3} \frac{dA_3}{dy} \Big|_{y=r_{ic}} \\ \frac{1}{\mu_3} \frac{dA_3}{dy} &= \frac{1}{\mu_4} \frac{dA_4}{dy} \Big|_{y=r_{ig}} \\ \frac{1}{\mu_4} \frac{dA_4}{dy} &= \frac{1}{\mu_5} \frac{dA_5}{dy} \Big|_{y=r_{im}} \end{aligned} \quad (36)$$

The form of the solution of the magnetic field control equation for each layer of (9) into (36) as follows:

$$\begin{cases}
 D_1 e^{-mr_{io}} = C_2 e^{\lambda r_{io}} + D_2 e^{-\lambda r_{io}} \\
 C_2 e^{\lambda r_{ic}} + D_2 e^{-\lambda r_{ic}} = C_3 e^{mr_{ic}} + D_3 e^{-mr_{ic}} \\
 C_3 e^{mr_{ig}} + D_3 e^{-mr_{ig}} = C_4 e^{mr_{ig}} + D_4 e^{-mr_{ig}} - \frac{iB_r}{m} \\
 C_4 e^{mr_{im}} + D_4 e^{-mr_{im}} - \frac{iB_r}{m} = C_5 e^{mr_{im}} \\
 -\frac{1}{\mu_1} D_1 m e^{-mr_{io}} = \frac{1}{\mu_2} [C_2 \lambda e^{\lambda r_{io}} - D_2 \lambda e^{-\lambda r_{io}}] \\
 \frac{1}{\mu_2} [C_2 \lambda e^{\lambda r_{ic}} - D_2 \lambda e^{-\lambda r_{ic}}] = \frac{1}{\mu_3} [C_3 m e^{mr_{ic}} - D_3 m e^{-mr_{ic}}] \\
 \frac{1}{\mu_3} [C_3 m e^{mr_{ig}} - D_3 m e^{-mr_{ig}}] = \frac{1}{\mu_4} [C_4 m e^{mr_{ig}} - D_4 m e^{-mr_{ig}}] \\
 \frac{1}{\mu_4} [C_4 m e^{mr_{im}} - D_4 m e^{-mr_{im}}] = \frac{1}{\mu_5} C_5 m e^{mr_{im}}
 \end{cases} \tag{37}$$

The value of each coefficient can be determined by solving the system of equations in (37).

REFERENCES

[1] Y. L. Wang, B. Zhang, and W. J. Deng, "Structure, characteristics and performance analysis of magnet eddy current flexible drive," *J. Magn. Mater. Devices*, vol. 47, no. 6, pp. 63–67, Nov. 2016, doi: 10.3969/j.issn.1001-3830.2016.06.014.

[2] C. J. Yang, C. L. Ji, and X. W. Zhang, "Torque and adjustable-speed relation for drum-type asynchronous magnetic couplers," *Electr. Mach. Control*, vol. 23, no. 1, pp. 108–116, Jan. 2019, doi: 10.15938/j.emc.2019.01.013.

[3] A. Wallace, A. von Jouanne, R. Jeffries, E. Matheson, and X. Zhou, "Comparison testing of an adjustable-speed permanent-magnet eddy-current coupling," in *Proc. Conf. Rec. Annu. Pulp Paper Ind. Tech. Conf.*, Atlanta, GA, USA, Jun. 2000, pp. 73–78, doi: 10.1109/PAPCON.2000.854194.

[4] A. C. Smith, A. El-Wakeel, and A. Wallace, "Formal design optimization of PM drive couplings," in *Proc. Conf. Rec. IEEE Ind. Appl. Conf. 37th IAS Annu. Meeting*, Pittsburgh, PA, USA, vol. 1, Oct. 2002, pp. 205–211, doi: 10.1109/IAS.2002.1044089.

[5] A. C. Smith, H. Willsamson, N. Benhama, L. Counter, and J. M. Papadopoulos, "Magnetic drive couplings," *Proc. 9th Int. Conf. Electr. Mach. Drives*, Canterbury, U.K., 1999, pp. 232–236, doi: 10.1049/cp:19991025.

[6] A. Wallace, A. von Jouanne, S. Williamson, and A. Smith, "Performance prediction and test of adjustable, permanent-magnet, load transmission systems," in *Proc. Conf. Rec. IEEE Ind. Appl. Conf. 36th IAS Annu. Meeting*, Chicago, IL, USA, vol. 3, Sep./Oct. 2001, pp. 1648–1655, doi: 10.1109/IAS.2001.955755.

[7] Y. Chaojun, "Mechanical properties and adjustable-speed characteristics of axial-flux-solid-type asynchronous magnetic couplers," *Electr. Mach. Control*, vol. 23, no. 5, pp. 110–118, May 2019, doi: 10.15938/j.emc.2019.05.014.

[8] G. Yongyong, "Research on characteristics of air gap of speed-regulation magnet coupler under condition of constant load," *J. Mine Autom.*, vol. 43, no. 11, pp. 74–79, Oct. 2017, doi: 10.13272/j.issn.1671-251x.2017.11.015.

[9] S. Jianwen, S. Ke, and M. State, "Analysis on influence factors of variable speed permanent magnetic coupler for mine," *J. Mining Sci. Technol.*, vol. 3, no. 01, pp. 68–75, Feb. 2018, doi: 10.19606/j.cnki.jmst.2018.01.009.

[10] D. Ioepp, *Ninth International Conference on Electrical Machines and Drives: Venue, Canterbury Christ Church College*. UKidge, U.K. Institution of Electrical Engineers, 1999.

[11] A. Canova and B. Vusini, "Design of axial eddy-current couplers," *IEEE Trans. Ind. Appl.*, vol. 39, no. 3, pp. 725–733, May/Jun. 2003, doi: 10.1109/TIA.2003.811783.

[12] A. Canova and B. Vusini, "Analytical modeling of rotating eddy-current couplers," *IEEE Trans. Magn.*, vol. 41, no. 1, pp. 24–35, Jan. 2005, doi: 10.1109/TMAG.2004.839730.

[13] S. Mohammadi, M. Mirsalim, S. Vaez-Zadeh, and H. A. Talebi, "Design analysis of a new axial-flux interior permanent-magnet coupler," in *Proc. 5th Annu. Int. Power Electron., Drive Syst. Technol. Conf. (PEDSTC)*, Tehran, Iran, Feb. 2014, pp. 562–567, doi: 10.1109/PEDSTC.2014.6799437.

[14] S. Mohammadi, M. Mirsalim, and S. Vaez-Zadeh, "Nonlinear modeling of eddy-current couplers," *IEEE Trans. Energy Convers.*, vol. 29, no. 1, pp. 224–231, Mar. 2014, doi: 10.1109/TEC.2013.2288948.

[15] T. Lubin and A. Rezzoug, "Steady-state and transient performance of axial-field eddy-current coupling," *IEEE Trans. Ind. Electron.*, vol. 62, no. 4, pp. 2287–2296, Apr. 2015, doi: 10.1109/TIE.2014.2351785.

[16] N. Bianchi, S. Bolognani, and E. Fornasiero, "An overview of rotor losses determination in three-phase fractional-slot PM machines," *IEEE Trans. Ind. Appl.*, vol. 46, no. 6, pp. 2338–2345, Nov./Dec. 2010, doi: 10.1109/TIA.2010.2070472.

[17] D. Colton, *Partial Differential Equations*. Mineola, NY, USA: Dover, 1988.

[18] N. Ida, *Engineering Electromagnetics*. 2021.

[19] G. B. Arfken, H. J. Weber, and F. E. Harris, *Mathematical Methods for Physicists*, 7th ed. 2012.

[20] J. B. Conway, *[Graduate Texts in Mathematics] Functions of One Complex Variable*, vol. 11. 1973, doi: 10.1007/978-1-4615-9972-2.

[21] R. L. Russell K. H. Norsworthy, "Eddy currents and wall losses in screened-rotor induction motors," *Proc. IEE-A, Power Eng.*, vol. 105, no. 20, pp. 163–175, 1958, doi: 10.1049/pi-a.1958.0036.

WANG TENG was born in Xinjiang, Shanxi, China, in 1964. He received the Ph.D. degree in engineering from Xi'an Jiaotong University, China, in 2006. He is currently with CCTEG Taiyuan Research Institute Company Ltd. He is also a researcher. His research interests include coal mine machinery design theory, mechanical system dynamics, and control technology.

WANG ZHENGHUI received the bachelor's degree in mechanical engineering from the China University of Mining and Technology, in 2020. He is currently pursuing the master's degree with the School of Mechanical Engineering, China Coal Research Institute, Beijing, China. His research interests include permanent magnet eddy current drive, fluid power transmission, and their application in coal mine machinery.

WU YIPENG received the bachelor's degree in traffic engineering from Tongji University, in 2020. He is currently pursuing the master's degree with the Department of Mechanical Engineering, China Coal Research Institute, Beijing, China. His research interests include permanent magnet eddy current drive, computational fluid dynamics, and their application in coal mine machinery.

GUO WENXIAO was born in Wenxi, Shanxi, China, in 1984. He received the Ph.D. degree in engineering from the North University of China, China, in 2021. He is currently with CCTEG Taiyuan Research Institute Company Ltd. He is also an associate researcher.

...